

Cognition and Behavior

# Dynamics of Visual Perceptual Decision-Making in Freely Behaving Mice

Wen-Kai You (游文愷)<sup>1,2</sup> and Shreesh P. Mysore<sup>1,2</sup><https://doi.org/10.1523/ENEURO.0161-21.2022><sup>1</sup>Department of Psychological and Brain Sciences, Johns Hopkins University, Baltimore, MD 21205 and <sup>2</sup>The Solomon H. Snyder Department of Neuroscience, Johns Hopkins University, Baltimore, MD 21205

## Abstract

The temporal dynamics of perceptual decisions offer a key window into the cognitive processes contributing to decision-making. Investigating perceptual dynamics in a genetically tractable animal model can facilitate the subsequent unpacking of the underlying neural mechanisms. Here, we investigated the time course as well as fundamental psychophysical constants governing visual perceptual decision-making in freely behaving mice. We did so by analyzing response accuracy against reaction time (RT), i.e., conditional accuracy, in a series of two-alternative forced choice (2-AFC) orientation discrimination tasks in which we varied target size, luminance, duration, and presence of a foil. Our results quantified two distinct stages in the time course of mouse visual decision-making: a “sensory encoding” stage in which conditional accuracy exhibits a classic trade-off with response speed, and a subsequent “short-term memory (STM)-dependent” stage in which conditional accuracy exhibits a classic asymptotic decay following stimulus offset. We estimated the duration of visual sensory encoding as 200–320 ms across tasks, the lower bound of the duration of STM as ~1700 ms, and the briefest duration of visual stimulus input that is informative as  $\leq 50$  ms. Separately, by varying stimulus onset delay, we demonstrated that the conditional accuracy function (CAF) and RT distribution can be independently modulated, and found that the duration for which mice naturally withhold from responding is a quantitative metric of impulsivity. Taken together, our results establish a quantitative foundation for investigating the neural circuit bases of visual decision dynamics in mice.

**Key words:** decision-making; dynamics; freely-behaving; mouse; perceptual; visual

## Significance Statement

This study presents a quantitative breakdown of the time course of visual decision-making in mice during naturalistic behavior. It demonstrates parallel stages in mouse visual perceptual decision dynamics to those in humans, estimates their durations, and shows that mice are able to discriminate well under challenging visual conditions, with stimuli that are brief, low luminance, and small. These results set the stage for investigating the neural bases of visual perceptual decision dynamics and their dysfunction in mice.

## Introduction

Exploring the temporal dynamics of perceptual decisions from onset of the sensory input through the initiation of behavioral responses affords a key window into the underlying cognitive processes (Uchida et al., 2006; Stanford et al., 2010; Siegel et al., 2011). Investigations of such dynamics in humans (Steinemann et al., 2018;

Wilming et al., 2020) and other species (Yang et al., 2008; Zariwala et al., 2013; Thura and Cisek, 2014) have revealed distinct stages in perceptual processing, their timing, and their interactions (Wickelgren, 1977; McElree and Doshier, 1989; Heitz, 2014). Performing such investigations in a genetically tractable animal model can additionally facilitate the subsequent unpacking of the mechanistic basis of

Received April 13, 2021; accepted February 17, 2022; First published February 28, 2022.

The authors declare no competing financial interests.

Author contributions: W.-K.Y. and S.P.M. designed research; W.-K.Y. performed research; W.-K.Y. analyzed data; W.-K.Y. and S.P.M. wrote the paper.

different stages in perceptual dynamics. However, despite the recent rise in the use of the laboratory mouse for the study of the visual system (Huberman and Niell, 2011; Glickfeld et al., 2014; Seabrook et al., 2017) and of visually guided decision-making (Prusky et al., 2000; Prusky and Douglas, 2004; Busse et al., 2011; Histed et al., 2012; Carandini and Churchland, 2013; Glickfeld et al., 2013; Long et al., 2015; Burgess et al., 2017; Wang and Krauzlis, 2018; Speed et al., 2020; You and Mysore, 2020), the temporal dynamics of visual perceptual decisions represents a significant gap in mouse visual psychophysics (Histed and Maunsell, 2014; Umino et al., 2018; Nomura et al., 2019).

In this study, we adapted approaches from human psychophysical studies to investigate the dynamics of visual decision-making in freely behaving mice. In a series of experiments involving touchscreen-based (Mar et al., 2013; You and Mysore, 2020), two-alternative forced choice (2-AFC) orientation discrimination tasks, we investigated the effect of stimulus size, luminance, duration, delay, and the presence of a competing foil on mouse decision performance [accuracy and reaction time (RT)], and importantly, on the conditional accuracy function (CAF). We identified two distinct stages in the time course of mouse visual decision-making within a trial, as has been reported in humans (Posner and Keele, 1967; Phillips and Baddeley, 1971; Dick, 1974; Coltheart, 1980; Shibuya and Bundesen, 1988; Busey and Loftus, 1994; Vogal et al., 2006; Bays et al., 2011). In the first “sensory encoding” stage (Shibuya and Bundesen, 1988; Busey and Loftus, 1994; Vogal et al., 2006; Bays et al., 2011), response accuracy exhibited a classic trade-off with response speed, and asymptoted to a peak level. In the next stage, response accuracy did not exhibit such a trade-off, but instead, decayed following stimulus offset, consistent with a classic short-term memory (STM)-dependent process (Posner and Keele, 1967; Phillips and Baddeley, 1971; Dick, 1974; Coltheart, 1980). Combining these results with those from drift diffusion modeling (DDM; Ratcliff et al., 2016) allowed us to estimate fundamental psychophysical constants in mouse perceptual decision-making: the time needed by mice to complete visual sensory encoding, the duration for which their STM can intrinsically support discrimination behavior after stimulus input is removed, and the shortest visual stimulus duration that is informative. Additionally, by varying stimulus onset delay, we demonstrated that the two components of accuracy, namely, the CAF and the RT distribution can be independently modulated by

task parameters. This also allowed a quantitative estimation of impulsivity of mice. Together, this study reveals parallels between mouse and human visual decision dynamics, despite differences in their sensory apparatuses, and enable investigations into the neural circuit underpinnings of the time course of perceptual decision-making in mice.

## Materials and Methods

### Animals

Thirty-seven mice (33 C57B16/J mice, all male; four PV-Cre mice, three female; The Jackson Laboratory) were housed in a temperature-controlled ( $\sim 75^\circ\text{F}$ ) and humidity-controlled ( $\sim 55\%$ ) facility on a 12/12 h light/dark cycle; zeitgeber time (ZT)0 = 7 A.M. All procedures followed the NIH guidelines and were approved by the Johns Hopkins University Animal Care and Use Committee (ACUC). Animals were allowed to acclimate for at least one week, with *ad libitum* access to food and water before water regulation was initiated per previously published procedures (Guo et al., 2014). Briefly, mice were individually housed (for monitoring and control of daily water intake of each identified animal), and administered 1 ml of water per day to taper their body weight down, over the course of 5–7 d, to 80–85% of each animal’s free-feeding baseline weight. During behavioral training/testing, the primary source of water for mice was as a reinforcer for correct performance: 10  $\mu\text{l}$  of water was provided for every correct response. Experiments were all conducted in the light phase.

### Apparatus

Behavioral training and testing were performed in sound-proof operant chambers equipped with a touchscreen (Med Associates Inc.), a custom-built reward port (fluid well), infrared video cameras, a house light and a magazine light above the reward port. The reward port was located at the opposite wall of the chamber relative to the touchscreen (Fig. 1A; Extended Data Fig. 1-1A). Mice were placed within a clear Plexiglas tube (5 cm in diameter) that connects the touchscreen and the reward port. A thin Plexiglas mask (3-mm thickness) was placed 3 mm in front of the touchscreen with three apertures (1 cm in diameter) through which mouse was allowed to interact with the screen via nose-touch. The “left” and “right” apertures were placed 3 cm apart (center-to-center) along the base of the triangle, and a “central” aperture, at the apex of the triangle, was 1.5 cm below the midpoint of the base. All experimental procedures were executed using control software (K-limbic, Med Associates).

### Visual stimuli

Visual stimuli were bright objects on the dark background (luminance =  $1.32\text{ cd/m}^2$ ). A small cross ( $60 \times 60$  pixels; luminance =  $130\text{ cd/m}^2$ ) was presented in the central aperture and had to be touched to initiate each trial. Oriented gratings (horizontal or vertical) were generated using a square wave, with fixed spatial frequency (24 pixel/cycle,  $\sim 0.1$  cycle/degree from 2 cm viewing distance, Extended Data Fig. 1-1A) known to be effective for mice to discriminate (Histed et al., 2012). The dark phase

This work was supported by the National Institutes of Health Grant R03 HD093995 and by startup funds from the Johns Hopkins University.

Acknowledgements: We thank James Garmon for help with fabrication of custom equipment.

Correspondence should be addressed to Shreesh P. Mysore at [mysore@jhu.edu](mailto:mysore@jhu.edu).

<https://doi.org/10.1523/ENEURO.0161-21.2022>

Copyright © 2022 You and Mysore

This is an open-access article distributed under the terms of the Creative Commons Attribution 4.0 International license, which permits unrestricted use, distribution and reproduction in any medium provided that the original work is properly attributed.

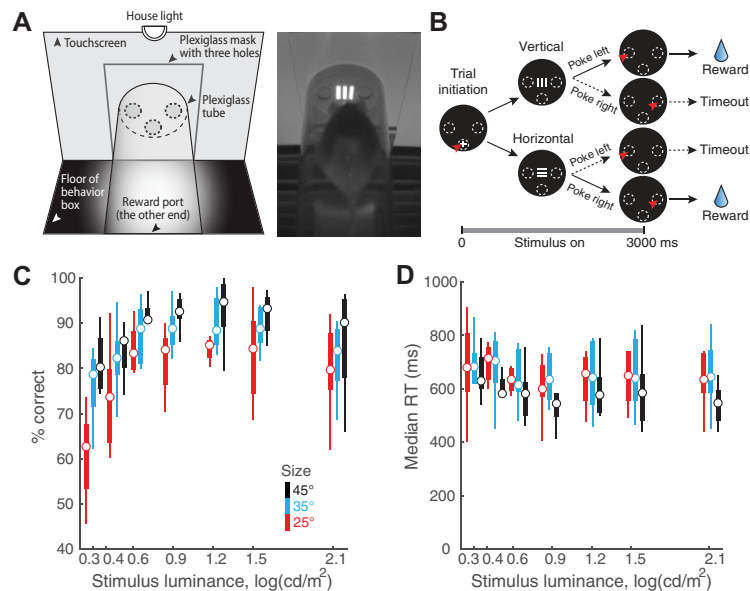


**Figure 1.** Stimulus luminance and size modulate orientation discrimination performance in freely behaving mice. **A**, Left, Schematic of touchscreen-based experimental setup showing key components. Right, Snapshot of freely behaving mouse facing a visual stimulus on the touchscreen. **B**, Schematic of 2-AFC task design. Black discs, Screenshots of touchscreen with visual stimuli. Dashed ovals, Locations of holes through which mice can interact with touchscreen; white “+”: zeroing cross presented within central response hole at start of each trial. Red arrowhead, Nose-touch by mouse. Shown also are vertical or horizontal grating stimuli, and reinforcement (water)/punishment (timeout) schedule. Bottom, Trial timeline. 0 ms corresponds to the instant at which the mouse touches the zeroing cross (trial initiation). Immediately following this, the target grating was presented and stayed on for 3 s, or until the mouse responded, whichever came first. Vertical and horizontal targets were interleaved randomly. **C**, Psychometric plots of discrimination accuracy against stimulus luminance ( $n=8$  mice). Different colors correspond to different target sizes. Two-way ANOVA,  $p < 0.001$  (luminance),  $p < 0.001$  (size),  $p = 0.498$  (interaction). Effect size  $\eta^2 = 0.292$  (luminance),  $\eta^2 = 0.192$  (size),  $\eta^2 = 0.037$  (interaction). For each stimulus size/luminance, the box plot shows the median (the central mark) and the 25th and 75th percentiles (the bottom and top edge of the box) of the group ( $n=8$ ). The whiskers extend to the most extreme data points not considered as outliers. **D**, Plot of median RT against stimulus luminance. Two-way ANOVA,  $p = 0.998$  (luminance),  $p = 0.004$  (size),  $p = 1$  (interaction). Effect size  $\eta^2 = 0.003$  (luminance),  $\eta^2 = 0.071$  (size),  $\eta^2 = 0.010$  (interaction).

of the grating was black, identical to the background (luminance,  $L_{\text{dark}} = 1.32 \text{ cd/m}^2$ ), and the bright phase was varied between 1.73 and 130  $\text{cd/m}^2$  depending on the tasks (see below). Note that as the luminance of the bright phase of the grating changed, the contrast of the grating also changed. For clarity, we refer to this stimulus manipulation as a change in luminance, throughout. The size of the stimulus was also varied depending on the task, ranging from  $60 \times 60$  to  $108 \times 108$  pixels, which subtended 25–45 visual degrees at a viewing distance of 2 cm from the screen (Extended Data Fig. 1-1A).

### Experimental procedure and behavioral training

Each mouse was run for one 30-min behavioral session per day, with each session yielding 80–180 trials. Each trial in a session was initiated by the mouse touching the zeroing cross. Upon trial initiation, the cross vanished, and the visual stimulus (or stimuli) were immediately presented (except in the delay task), for a duration of 0.1–3 s depending on the task (see below). Mice were trained to report the orientation of target grating, by nose-touching the correct response aperture (vertical  $\rightarrow$  left; horizontal  $\rightarrow$  right). A correct response triggered a tone (600 Hz, 1 s), the magazine light turning on, and the delivery of 10  $\mu\text{l}$  of water. When mice turned to consume the reward, their head entry into the reward

port was detected by an infrared sensor which caused the zeroing cross (for the next trial) to be presented again. An incorrect response triggered a 5-s timeout, during which the house light and the magazine light were both on and zeroing cross was unavailable for the next trial to be initiated. A failure to respond within 3 s (starting stimulus presentation) resulted in a trial reset: the stimulus vanished and the zeroing cross was presented immediately (without a timeout penalty), to allow initiation of the next trial. Well-trained animals failed to respond on fewer than 5% of the total number of trials, and there were no systematic differences in the proportion of such missed trials between different conditions. Within each daily 30-min behavioral session, mice consumed  $\sim 1$  ml of water. If a mouse failed to collect enough water from the behavioral session, they were provided with a water supplement using a small plastic dish in their home cage.

### Single-stimulus discrimination task

Upon trial initiation, a single grating stimulus (i.e., the “target”) was presented above the central aperture, at the same horizontal level as the left and right apertures, and mice were required to report its orientation with the appropriate nose-touch (Fig. 1B). When stimulus size and luminance were manipulated (Figs. 1, 2), three different sizes were tested:  $60 \times 60$ ,  $84 \times 84$ ,  $108 \times 108$  (pixels  $\times$

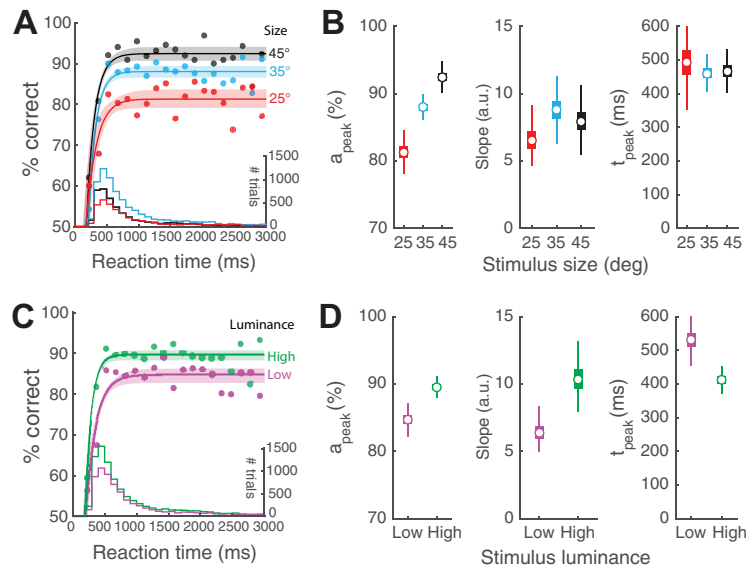


**Figure 2.** Stimulus size and luminance modulate the sensory encoding stage of the CAF. **A**, Plot of accuracy as a function of RT bins (conditional accuracy) using same dataset as Figure 1. Data pooled across all stimulus luminance and mice ( $n=8$ ), sorted by stimulus size; RT bin size = 100 ms. Solid curves, CAFs (best-fit rising asymptotic function; Materials and Methods) for targets of different sizes (black: 45°; blue: 35°; red: 25°). Light shading, 95% confidence interval of the fit (abbreviated as C.I., henceforth; Materials and Methods). Histograms at bottom, RT distributions for targets of different sizes (y-axis on the right). The overall response accuracy for a particular stimulus condition is the dot product of the CAF and the RT distribution. **B**, Box plots of the key parameters for different target sizes. Left panel,  $a_{peak}$ . Middle panel, Slope parameter. Right panel,  $t_{peak}$ . **C**, CAFs for targets of different luminance conditions (magenta: “low” luminance, first three luminance levels from Fig. 1C; green: “high” luminance, last four luminance levels; Materials and Methods); conventions as in **A**. **D**, Box plots of the key parameters for different luminance conditions; conventions as in **B**. The box plots in all panels show the median (open circle), the 25th and 75th percentiles (the bottom and top edge of the box), and the most extreme data points not considered as outliers (whiskers); in some panels, the boxes are the same size as the symbol for the median.

pixels). For each size, seven different levels of luminance were tested: 2.00, 2.59, 4.37, 7.55, 16.2, 34.3, 130  $\text{cd}/\text{m}^2$ . [These corresponded nominally to Michelson’s contrasts of 20%, 32%, 54%, 70%, 85%, 93%, 98%, respectively; Michelson’s contrast is computed as  $(\text{luminance}_{\text{bright}} - \text{luminance}_{\text{dark}}) / (\text{luminance}_{\text{bright}} + \text{luminance}_{\text{dark}}) \times 100$ .] Trials with different stimulus luminance at a particular size were interleaved randomly throughout a session, while trials with different stimulus sizes were examined on different days. When the stimulus duration was manipulated (Fig. 3), the luminance (130  $\text{cd}/\text{m}^2$ ) and size (60  $\times$  60 pixels) of the grating were fixed, and eleven different stimulus durations were tested: 100, 200, 300, 400, 500, 600, 800, 1000, 1500, 2000, 3000 ms. The stimulus duration was fixed for a given day, and across days, was varied in a descending sequence from 3000 to 100 ms. When the stimulus onset delay was manipulated, the luminance (130  $\text{cd}/\text{m}^2$ ), size (60  $\times$  60 pixels), and duration (600 ms) of the grating were fixed. Three different delays were tested: 0, 100, and 200 ms. The delay duration was fixed for a given day, and varied in an ascending sequence from 0 to 200 ms.

### Flanker task

Upon trial initiation, either one stimulus (“target,” 60  $\times$  60 pixels, luminance = 20.1  $\text{cd}/\text{m}^2$ ) was presented at the lower location, or two stimuli were presented simultaneously, with the target at the lower location and a second “flanker” at the upper location (Fig. 4A). Flankers were of the same

size (60  $\times$  60 pixels) and spatial frequency (24 pixels/cycle) as the target, but with luminance ranging (over eight levels) from less than that of the target to greater than that of the target (You and Mysore, 2020). The orientation of the flanker was either identical to that of the target (“congruent trial”) or orthogonal to that of the target (“incongruent trial”). The stimulus (stimuli) was (were) presented for a duration of 1 s, and mice were required to report orientation of the target grating with the appropriate nose-touch (within 3 s). All types of trials (no flanker, congruent, incongruent) and flanker luminance were interleaved randomly within each daily session. Data from this experiment have been reported previously (You and Mysore, 2020), and were re-analyzed here using different analyses.

### Subject inclusion/exclusion

A total of 37 mice were used in this study, with different subsets used in different tasks. For mice involved in more than one task, they were well rested for three to eight weeks with food and water *ad libitum* between experiments. Before the start of each experiment, all mice were given a few days of practice session to ensure that they remembered/re-learned the association between the orientation of single target and the appropriate nose-touch. Of the total of 37 mice trained across tasks, 28 mice passed the inclusion threshold of response accuracy >70% in the single-stimulus

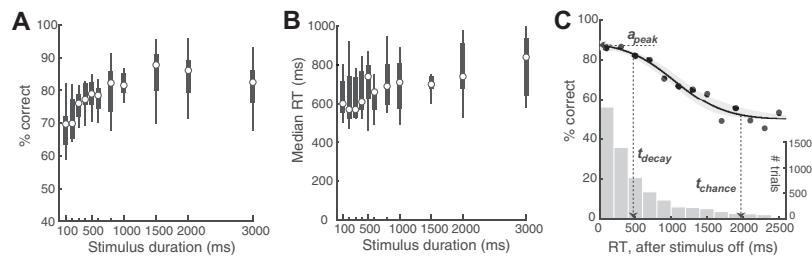


**Figure 3.** Stimulus duration and the memory-dependent stage of the CAF. **A**, Psychometric plot of discrimination accuracy against stimulus duration ( $n=9$  mice; one-way ANOVA;  $p < 0.001$ ; effect size  $\eta^2 = 0.331$ ). **B**, Plot of median RT against stimulus duration (one-way ANOVA;  $p = 0.056$ ; effect size  $\eta^2 = 0.177$ ). **C**, Plot of the conditional accuracy (solid data) as a function of RT bins relative to stimulus offset. Only trials in which the stimulus was longer than 332 ms were included (to ensure full sensory encoding, see text; Materials and Methods). Curve and shading, Best-fit sigmoid function and 95% C.I. Bootstrapped estimates of each key metric:  $a_{\text{peak}}$ , median [C.I.] = 87.3 [84.8, 89.9] %;  $t_{\text{decay}} = 469$  [279, 697] ms; and  $t_{\text{chance}} = 1969$  [1708, 2520] ms. Histogram, RT distribution ( $y$ -axis on the right). In this experiment, stimulus size and luminance were maintained fixed at  $25^\circ$  and  $130 \text{ cd/m}^2$ , respectively.

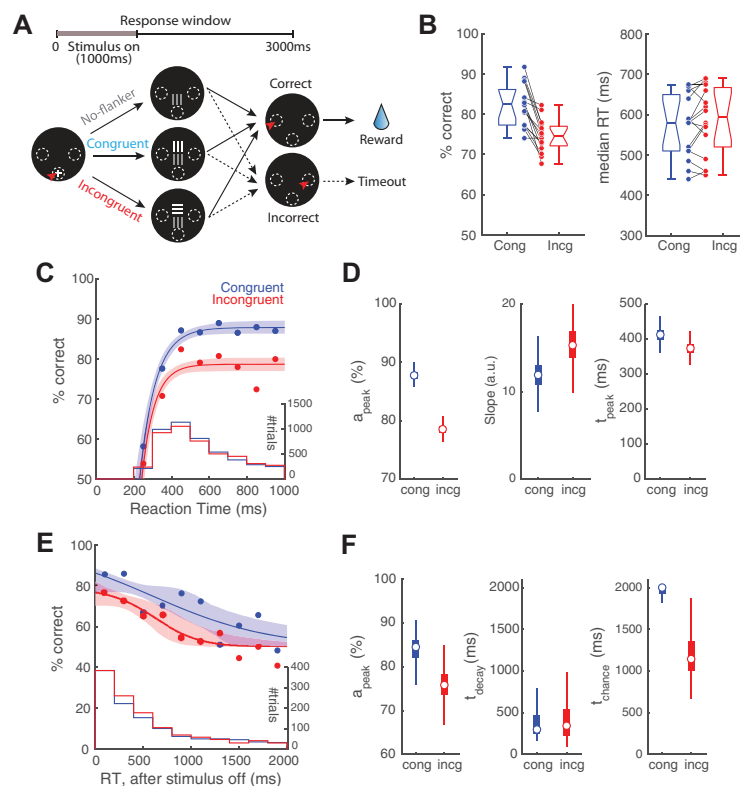


**Figure 4.** Incongruent flanker modulates the sensory encoding stage of the CAF. **A**, Schematic of the flanker task; target grating is always presented at the lower location; a second “flanker” grating (orthogonal orientation, incongruent flanker; or same orientation, congruent flanker) is presented simultaneously, and always at the upper location; luminance of flanker is systematically varied (adapted from You and Mysore, 2020). All other conventions as in Figure 1. The stimuli were presented for 1 s, and the response window was 3 s. **B**, Left panel, Comparison of performance between trials with incongruent versus congruent flanker.  $p < 0.001$ , paired-sample  $t$  test. Effect size Hedges’  $g = 1.61$ . Right panel, Comparison of median RT between trials with incongruent versus congruent flanker.  $p = 0.137$ , paired-sample  $t$  test. Effect size Hedges’  $g = -0.176$ . Data re-analyzed from You and Mysore (2020); each line represents data from one mouse ( $n = 17$  mice). Data in **B–F** include only trials with high flanker luminance ( $\geq 20.1 \text{ cd/m}^2$ ; see text). **C**, CAFs of the sensory encoding stage. Blue, Trials with congruent flanker. Red, Trials with incongruent flanker. Histograms, RT distributions. **D**, Key parameters of CAFs (sensory encoding stage) for trials with congruent versus incongruent flanker;  $a_{\text{peak}}$  (left), slope parameter (middle), and  $t_{\text{peak}}$  (right). Box plots show the distribution of bootstrapped estimates (Materials and Methods). Effect sizes (congruent–incongruent):  $a_{\text{peak}}$ : Hedges’  $g = 11.0$ ; slope parameter: Hedges’  $g = -1.73$ ;  $t_{\text{peak}}$ : Hedges’  $g = 2.08$ . Note, the sizes of the boxes in the left and right panels are similar to the sizes of the circular symbols depicting the medians. **E**, CAFs of the STM-dependent stage; data aligned to stimulus offset. Blue, Trials with congruent flanker. Red, Trials with incongruent flanker. **F**, Plots of key parameters of CAFs (STM-dependent stage) for trials with congruent versus incongruent flanker;  $a_{\text{peak}}$  (left),  $t_{\text{decay}}$  (middle), and  $t_{\text{chance}}$  (right). Conventions and statistical methods as in **D**.  $a_{\text{peak}}$ : Hedges’  $g = 2.54$ ;  $t_{\text{decay}}$ : Hedges’  $g = 0.175$ ;  $t_{\text{chance}}$ : Hedges’  $g = 2.98$ .

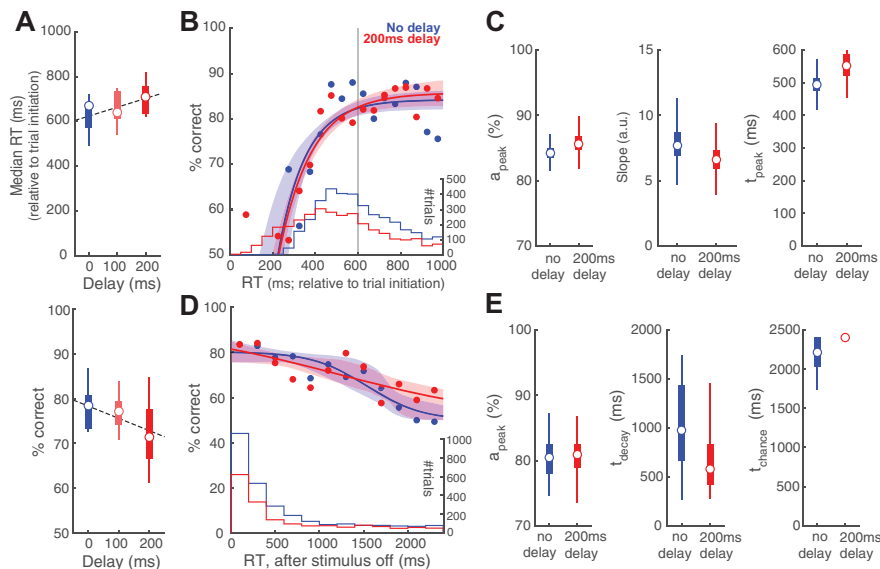


**Figure 5.** Stimulus onset delay modulates RT distribution but not the CAF. **A**, Upper, Plot of median RT, measured relative to trial initiation, against stimulus onset delay ( $n=9$  mice;  $p=0.094$ , one-way ANOVA; effect size  $\eta^2 = 0.179$ ; Pearson's correlation = 0.422,  $p=0.028$ ). Dashed line, Linear regression on RTs. Lower, Plot of response accuracy against stimulus onset delay ( $p=0.182$ , one-way ANOVA; effect size  $\eta^2 = 0.132$ ; Pearson's correlation =  $-0.358$ ,  $p=0.067$ ). **B**, CAFs of the sensory encoding stage. Blue, Trials with no delay. Red, Trials with 200-ms delay. Shaded bands, Bootstrapped confidence intervals (95%); confidence intervals overlap for the two datasets. Histograms, RT distributions. Gray vertical line, Stimulus offset. **C**, Key parameters of the CAF (sensory encoding stage) for trials with no delay versus trials with 200-ms delay. Box plots show the distribution of the bootstrapped estimates. **D**, CAFs of the STM-dependent stage. Conventions as in **B**. **E**, Key parameters of the CAF (STM-dependent stage) for trials with no delay versus trials with 200-ms delay. Conventions as in **C**.

discrimination task, and were included for the analyses reported in this paper.

### Trial inclusion/exclusion

Mice were observed to become less engaged in the task toward the end of a behavioral session, when they had received a sizeable proportion of their daily water intake. This was reflected in their behavioral metrics: they tended to wait longer to initiate the next trial, and their performance deteriorated. We identified and excluded such trials following a published procedure (You and Mysore, 2020), to minimize confounds arising from loss of motivation toward the end of sessions. Briefly, we pooled data across all mice and all sessions, treating them as coming from one session of a single “mouse.” We then binned the data by trial number within the session, computed the discrimination accuracy in each bin (% correct), and plotted it as a function of trial number within session (Extended Data Figs. 1-1B, 3-1A, 5-1A). Using a bootstrapping approach, we computed the 95% confidence interval for this value. We used the following exclusion criterion: trials  $q$  and above were dropped if the  $q^{\text{th}}$  trial was the first trial at which at least one of the following two conditions was satisfied: (1) the performance was statistically indistinguishable from chance on the  $q^{\text{th}}$  trial and for the majority (3/5) of the next five trials (including the  $q^{\text{th}}$ ); (2) the number of observations in  $q^{\text{th}}$  trial was below 25% of the maximum possible number of observations for each trial ( $\Sigma$  mice  $\times$  sessions), thereby signaling substantially reduced statistical power available to reliably compare

performance to chance. The plots of performance as a function of trial number, and number of observations as a function of trial number for the different tasks in this study are shown in Extended Data Figures 1-1B, 3-1A, 5-1A, along with the identified cutoff trial numbers ( $q$ ).

### Behavioral measurements

Response accuracy (% correct) was calculated as the number of correct trials divided by the total number of trials responded (correct plus incorrect). RT was defined as the time between the start of stimulus presentation and time of response nose-touch, both detected by the touchscreen. In the experiment involving stimulus onset delays (Fig. 5A), RT was computed with respect to trial initiation (as opposed to from stimulus onset).

### DDM of RT distributions

The RT measured here represents the duration from stimulus onset to completion of the motor response. In order to specifically isolate the time spent in decision-making (separately from the latency of activation of sensory neurons as well as duration of motor execution), we applied the drift-diffusion model to our RT data (Voss et al., 2013, 2015). This model hypothesizes that a subject (“decision-maker”) collects information from the sensory stimulus via sequential sampling, causing sensory evidence to accrue for or against a particular option (usually binary) while viewing the stimulus. A decision is to be made when the accumulating evidence reaches an internal threshold of the subject. This process of evidence

accumulation, together with the processes of sensory encoding and motor execution, as well as threshold crossing, determine the RT observed on each trial.

We used a standard version of the model that consists of four independent variables (Ratcliff, 1978; Ratcliff et al., 2016): (1) the drift rate; (2) the boundary separation; (3) the starting point; and a (4) nondecisional constant ( $t_{\text{delay}}$ ), which accounts for the time spent in sensory transmission and motor execution. In the case of our tasks, there was no reason for the drift rate to be different between vertical versus horizontal gratings, and therefore, we merged both type of trials (trials with a horizontal target grating and trials with a vertical target grating). We treated “correct” response and “incorrect” response as the two binary options, and fit the diffusion model to the RT distributions of correct versus incorrect trials using the fast-dm-30 toolbox with the maximum likelihood option to gain estimates of those four parameters for each individual mouse (Extended Data Fig. 2-2; Voss et al., 2015).

### Conditional accuracy analysis

Conditional accuracy was calculated as the percentage of correct trials (accuracy) as a function of RT. For this analysis, trials from all mice were pooled together and treated as if they were from one single mouse for statistical power (Fig. 2 onwards; for completeness, conditional accuracy plots using nonpooled data, i.e., from individual mice, are included in Extended Data Figs. 2-1A, 3-1B). Pooled trials were then sorted by their RT, and then binned by RT such that there were: (1) sufficient number of trials in each bin; and (2) sufficient number of total bins, to ensure the robustness of curve fitting and therefore the estimates of quantitative metrics (see below). Typical bin sizes used were 50-, 100-, or 200-ms bins, depending on the experiments and stage of analysis (sensory encoding or STM-dependent). The effect of bin size on the estimates of quantitative metrics is explored in the Extended Data Figures 2-1B-G, 3-1C-H; results show that the estimates are comparable across tested bin sizes.

### CAF

To quantitatively describe the relationship between the conditional accuracy and RT, we fitted the plot of accuracy against binned RT with parametric functions (the CAF; see below) using a nonlinear least square method. For RT bins aligned to stimulus onset (Figs. 2, 4C, 5B), we fit the conditional accuracy data using an increasing asymptotic function:

$$\text{Conditional accuracy} = \lambda \left( 1 - e^{-\gamma_{\text{enc}}(\text{RT} - \delta)} \right).$$

Three key metrics were defined for this sensory encoding phase, for use in subsequent comparisons across conditions: (1) peak conditional accuracy ( $a_{\text{peak}}$ ), the maximal level of accuracy that the CAF reaches within the range of RT; (2) the slope parameter ( $\gamma_{\text{enc}}$ ); and (3) the first instant at which the conditional accuracy reaches its maximal value ( $t_{\text{peak}}$ ), defined as the time point at which the ascending CAF reaches 95% of  $a_{\text{peak}}$ . Note that  $t_{\text{peak}}$  is

influenced by the peak conditional accuracy ( $a_{\text{peak}}$ ), the slope parameter,  $\gamma_{\text{enc}}$ , and the temporal offset at chance performance,  $\delta$ . For RT bins aligned to stimulus offset (Figs. 3C, 4E, 5D), we fit the decaying conditional accuracy data using a sigmoidal function:

$$\text{Conditional accuracy} = \lambda [1 / (1 + e^{-\beta_{\text{dec}}(\text{RT} - \tau)})] + 50.$$

Three key metrics were defined for this STM-dependent stage for use in subsequent comparisons across conditions: (1) peak conditional accuracy ( $a_{\text{peak}}$ ), the maximal level of accuracy within the range of RT; (2) the first instant ( $t_{\text{decay}}$ ) at which conditional accuracy is lower than the maximum, defined as the time point at which the descending CAF crosses 95% of  $a_{\text{peak}}$ ; and (3) the first instant ( $t_{\text{chance}}$ ) at which conditional accuracy drops to chance level, defined as the time point at which the descending CAF crosses 52.5%. In (rare) cases when the CAF never went below 52.5%,  $t_{\text{chance}}$  was set to be the upper bound of the window of analysis (i.e., 3000 ms – stimulus duration = the window for which the mice can respond following stimulus offset). Note that  $t_{\text{decay}}$  and  $t_{\text{chance}}$  are influenced by both the slope parameter,  $\beta_{\text{dec}}$ , and  $\tau$ .

Confidence intervals of the CAF fits, as well as for the parameters, were estimated by standard bootstrapping procedures involving resampling the raw data randomly with replacement (1000×), to get repeated estimates of the CAF and corresponding metrics. In all relevant figures, the box plots of the estimated values of each metric show the median (the central mark), the 25th and 75th percentiles (the bottom and top edge of the box), and the most extreme data points not considered as outliers (whiskers).

In the experiment in which the stimulus onset delay was manipulated (Fig. 5), we adopted the following two adjustments to our procedure for the analysis of the CAF. First, since the stimulus was short (600 ms), to ensure robust estimates of CAF metrics for the sensory encoding stage, we included data beyond stimulus offset as well for the fitting of the CAF through 400 ms following offset. (We chose to include data up to 400 ms after offset, specifically, because we had learned from Fig. 3 that conditional accuracy remains at its plateau for nearly 500 ms following stimulus offset.) Second, we also excluded trials with  $\text{RT} < 200$  ms for the fitting of the CAF (Fig. 5B), because these represent trials on which responses were initiated prematurely, before the stimulus was even presented (200 ms represents our estimate of the duration of sensory latency plus motor execution; see text to Fig. 2).

### Statistical tests

All analyses and statistical tests were performed in MATLAB. For single-stimulus experiments in which only one stimulus parameter was systemically varied, one-way ANOVA was applied to examine the effect of the manipulating the single factor (duration and delay; Figs. 3A,B, 5A; Extended Data Fig. 1-1C,D). For experiments that involved changing both stimulus size and luminance (Fig. 1C,D; Extended Data Fig. 2-2), two-way ANOVA was applied to examine the effect of each factor, as well as their

interaction. For the flanker task, the paired-sample  $t$  test was used to examine whether the group performance was different between trial types (Fig. 4B).

For the metrics associated with CAF, comparisons were made by measuring the effect size (Hedges'  $g$ ) of the difference between two distributions (Figs. 2B,D, 4D,F, 5C,E). All effect size measurements, including those with ANOVA ( $\eta^2$ ), were calculated following the methods (and source code) of Hentschke and Stüttgen (2011). Hedges'  $g$  estimates the distance between the two distributions in units of their pooled standard deviation, with larger numbers indicating stronger effects.  $\eta^2$  varies from 0 to 1, with larger values indicating greater ratio of variance explained in the dependent variable by a predictor while controlling the other variables.

## Results

In this study, freely behaving mice were trained to perform 2-AFC orientation discrimination in a touchscreen-based setup (Mar et al., 2013; You and Mysore, 2020; Materials and Methods). Briefly, mice were placed in a Plexiglas tube within a soundproof operant chamber equipped with a touch-sensitive screen at one wall and a reward well at the opposite wall (Fig. 1A). A Plexiglas sheet with three holes was placed in front of the touchscreen, the holes corresponded to the locations at which mice were allowed to interact with the screen by a nose-touch (Fig. 1A). All trials began with a nose-touch on a bright zeroing-cross presented within the lower central hole (Fig. 1B). Immediately following nose-touch, an oriented grating (target; bright stimulus on a dark background) was presented at the center of the screen. Mice were rewarded if they responded to the orientation of the target with an appropriate nose-touch: vertical (horizontal) grating  $\rightarrow$  touch within upper left (upper right) hole. Behavioral data were collected from daily sessions that lasted 30 min for each mouse (see also Extended Data Fig. 1-1).

### Stimulus size and luminance modulate mouse discrimination performance

We first examined the effect of target size and luminance on the decision performance of mice in the orientation discrimination task. Here, the target grating was presented for up to 3 s after trial initiation (Fig. 1B; Materials and Methods), and its size and luminance were systematically varied; the spatial frequency was fixed at 0.1 cycles/degree (24 pixels/cycle; Prusky and Douglas, 2004; Histed et al., 2012; Materials and Methods). Mice were allowed to respond at any time during stimulus presentation, and the stimulus was terminated automatically on response.

We found that both the target luminance and size significantly modulated discrimination accuracy (two-way ANOVA, main effect of luminance,  $p < 0.001$ , effect size  $\eta^2 = 0.292$ ; main effect of size,  $p < 0.001$ ,  $\eta^2 = 0.192$ ; interaction,  $p = 0.498$ ,  $\eta^2 = 0.037$ ; Fig. 1C). These results revealed that mice discriminated target orientation better than chance even at the lowest luminance (2.00 cd/m<sup>2</sup>) and size (25°) tested (the red box at the left lower corner,

$p = 0.015$ ,  $t$  test against mean accuracy = 50%, effect size  $g_1 = 1.129$ ; Fig. 1C). Additionally, at this smallest target size (25°), mice could discriminate with >80% accuracy for most of the tested luminance values ( $\geq 4.37$  cd/m<sup>2</sup>; Fig. 1C, red data).

The effect of these parameters on median RTs was less pronounced. Target size, but not luminance, modulated RTs (two-way ANOVA; main effect of size,  $p = 0.004$ , effect size  $\eta^2 = 0.071$ ; main effect of luminance,  $p = 0.998$ ,  $\eta^2 = 0.003$ ; interaction,  $p = 1$ ,  $\eta^2 = 0.010$ ; Fig. 1D). Together, these results revealed a systematic effect of target size and luminance on discrimination accuracy.

### Effect of stimulus size and luminance on dynamics of visual decision-making: the sensory encoding stage

To investigate the dynamics of visual perceptual decision-making, we adapted approaches from human studies and examined the dependence of response accuracy on RT, i.e., the so-called CAF (Wickelgren, 1977; McElree and Doshier, 1989; Heitz, 2014). For these analyses, we pooled trials from all mice ( $n = 8$ ) to gain better statistical power for the estimates of parameters of the CAF (Materials and Methods; plots of the data for individual mice showed similar overall shapes of the CAF; Extended Data Fig. 2-1A).

Specifically, we investigated the dynamics of visual perceptual decision-making as a function of stimulus size, and separately, as a function of stimulus luminance. First, to examine the effect of stimulus size on decision dynamics, we pooled trials from all mice across luminance values (7 luminance values) for each stimulus size, sorted them based on RT, and plotted conditional accuracy for each RT bin (100 ms; Fig. 2A; Materials and Methods). We found that for responses with RT less than ~500 ms, conditional accuracy improved for longer RT, consistent with the classic "speed-accuracy trade-off" (Heitz, 2014). For responses with RT >500 ms and up to 3 s, the allowed duration for responses, conditional accuracy plateaued, and was independent of RT. Next, to examine the effect of stimulus luminance on decision dynamics, we pooled trials from all mice across size values into two groups based on stimulus luminance: (1) trials with target luminance  $\leq 4.37$  cd/m<sup>2</sup> ("low luminance"); and (2) trials with target luminance  $> 4.37$  cd/m<sup>2</sup> ("high luminance"; Materials and Methods). Here, as well, we found a similar initial stage of increasing conditional accuracy up to RT of ~500 ms, followed by a plateauing of conditional accuracy.

Drawing on arguments from human behavioral studies, we reasoned that the initial transient stage of the CAF reflects the process of sensory encoding: during it, slower responses allow more sensory evidence to be acquired, thereby improving conditional accuracy up to a peak value reflecting the completion of sensory encoding (Shibuya and Bundesen, 1988; Busey and Loftus, 1994; Vogel et al., 2006; Bays et al., 2011).

To quantify these dynamics, we fit the conditional accuracy data with an asymptotic function (Fig. 2A,C, solid curves; Wickelgren, 1977; McElree and Doshier, 1989; Heitz, 2014), and estimated three key metrics, in each



case: (1) the peak conditional accuracy ( $a_{\text{peak}}$ ); (2) the slope parameter ( $\gamma_{\text{enc}}$ ); and (3) the time point at which conditional accuracy reached its peak ( $t_{\text{peak}}$ ; Materials and Methods).

We found that the peak conditional accuracy was significantly modulated by stimulus size (Fig. 2B, left;  $a_{\text{peak}}$ : size 25°, median [95% confidence interval, C.I.] = 81.3 [79.1, 83.7] %; size 35° = 88.0 [86.5, 89.4] %; size 45° = 92.4 [90.7, 94.1] %; effect size Hedges'  $g = -6.71$  (25° versus 35°),  $-5.39$  (35° versus 45°),  $-10.6$  (25° versus 45°)), but not the slope of the function (slope parameter,  $\gamma_{\text{enc}}$ , Fig. 2B, middle; size 25° = 6.52 [5.10, 9.07] a.u.; size 35° = 8.81 [7.09, 10.6] a.u.; size 45° = 7.92 [6.15, 10.1] a.u.; Hedges'  $g = -2.24$  (25° versus 35°), 0.863 (35° versus 45°),  $-1.34$  (25° versus 45°)), or the time to reach peak accuracy ( $t_{\text{peak}}$ , Fig. 2B, right; size 25° = 493 [375, 597] ms; size 35° = 459 [420, 505] ms, size 45° = 466 [420, 522] ms; Hedges'  $g = 0.728$  (25° versus 35°),  $-0.274$  (35° versus 45°), 0.558 (25° versus 45°)).

Next, we found that the peak conditional accuracy was higher in high-luminance trials (Fig. 2D, left; low-luminance, median [C.I.] = 84.7 [82.7, 86.3] %; high-luminance = 89.5 [88.2, 90.7] %, effect size Hedges'  $g = -6.13$ ). The slope was also higher in high-luminance trials (slope parameter,  $\gamma_{\text{enc}}$ , Fig. 2D, middle; low-luminance = 6.37 [5.21, 7.78] a.u.; high-luminance = 10.32 [8.49, 12.6] a.u., Hedges'  $g = -4.51$ ) suggesting a faster rate of sensory encoding in high-luminance trials. Consistent with this, the time to reach peak accuracy was shorter in high-luminance trials (Fig. 2D, right;  $t_{\text{peak}}$ : low-luminance = 531 [478, 599] ms; high-luminance = 412 [378, 448] ms, Hedges'  $g = 4.86$ ).

The RT measured here represents the duration from the start of the sensory input to the completion of motor response. In order to obtain an estimate of the duration, specifically, of decision-making, we employed the standard DDM approach (Ratcliff, 1978; Ratcliff et al., 2016; Materials and Methods). Briefly, the DDM analyzes the full RT distribution and yields a quantitative estimate of four parameters (Materials and Methods), one of which is  $t_{\text{delay}}$ , a parameter which accounts for the combination of the following: (1) the time taken for the sensory (visual) periphery to transduce and relay information to visual brain areas (i.e., neural response latency); and (2) the time taken for executing the motor response (i.e., motor execution delay). In our tasks, the latter corresponds to the time for the mouse to move its head (and body) to achieve the appropriate nose-touch.

Using this approach, we found that stimulus size as well as luminance had no discernable effect on  $t_{\text{delay}}$  (two-way ANOVA, size:  $p = 0.308$ , luminance:  $p = 0.523$ ; interaction:  $p = 0.931$ ; Extended Data Fig. 2-2), and the average value of  $t_{\text{delay}}$  was 212 ms. Consequently, we estimated the duration of just the sensory encoding stage (temporal integration window) as  $t_{\text{peak}} - t_{\text{delay}} = t_{\text{peak}} - 212$  ms. Across conditions, this took values of 200 ms (412–212 ms; high luminance), 254 ms (466–212 ms; size of 45°), 247 ms (459–212 ms; size of 35°), 281 ms (493–212 ms; size of 25°), and 319 ms (531–212 ms, low luminance).

Thus, conditional accuracy analysis allowed us to quantify the sensory encoding stage in mouse visual

perceptual dynamics. We estimated its duration to be brief, varying between 200 and 320 ms across the tested conditions.

Following the completion of sensory encoding, a fully constructed representation of the sensory stimulus is available, as a result of which, additional sampling of the stimulus brings no extra benefits to the performance. Our finding that RTs longer than  $t_{\text{peak}}$  produce no further increase in conditional accuracy, is consistent with the view (Fig. 2A,C; see also Extended Data Figs. 2-1, 2-2).

### Stimulus duration and the dynamics of visual decision-making: the memory-dependent stage

The next stage in the time course of perceptual decisions has been identified in human studies as the so-called STM-dependent stage, during which an internal representation of the sensory stimulus is available transiently in memory for guiding behavior (Smith and Ratcliff, 2009). Studies have demonstrated the STM to be labile such that once the stimulus is terminated, sensory information maintained in STM decays and is lost (over seconds; Brown, 1958; Gold et al., 2005; Zhang and Luck, 2009; Barrouillet and Camos, 2012; Ricker et al., 2016).

In our experiments so far, the target stimulus was present on the screen for the full duration of the response window (3 s). Here, to investigate and quantify the STM-dependent stage of mouse perceptual decisions, we performed an experiment in which we shortened the stimulus duration systematically from 3 s to 100 ms. This allowed us to examine the time course of decision behavior following stimulus offset and to examine the shortest stimulus that mice are able to discriminate effectively.

We first examined overall mouse behavioral performance at different stimulus durations. We found that response accuracy was significantly modulated (one-way ANOVA,  $p < 0.001$ , effect size  $\eta^2 = 0.331$ ; Fig. 3A), with accuracy decreasing for shorter stimulus durations (Pearson's  $\rho = 0.712$ ,  $p = 0.014$ ). There was also a trend of decreasing median RT for shorter stimulus durations (one-way ANOVA,  $p = 0.056$ , effect size  $\eta^2 = 0.177$ ; Pearson's  $\rho = 0.861$ ,  $p = 0.001$ ; Fig. 3B). Additionally, these results revealed, that the shortest stimulus duration needed for mice to be able to discriminate above chance was  $< 100$  ms, the smallest duration tested (Fig. 3A; see also Extended Data Fig. 3-1).

Next, to examine the decision dynamics following stimulus offset, we aligned trials to stimulus offset, and computed the conditional accuracy. Considering that incomplete sensory encoding may be a confounding factor to the STM decay, we only included those trials on which the stimulus was presented for longer than the duration of the sensory encoding stage, estimated in Figure 2 to be 320 ms.

We observed the classic decay in conditional accuracy with longer RTs (Fig. 3C). To quantify the time course of the decay, we fit the conditional accuracy data with a sigmoidal function (Materials and Methods), and estimated three key metrics (Fig. 3C; Materials and Methods). The first, peak performance,  $a_{\text{peak}}$ , was 87.3% (median, C.I. = [84.8, 89.9] %), comparable to the asymptotic level of Figure 2, thereby supporting that sensory encoding is,

indeed, complete on these trials. The second, the time point at which the conditional accuracy dropped below the peak value,  $t_{\text{decay}}$ , was 469 ms (median, C.I. = [279, 697] ms) after stimulus offset. The third, the first time point at which the discrimination accuracy dropped to a level indistinguishable from the chance,  $t_{\text{chance}}$ , was 1969 ms (median, C.I. = [1708, 2520] ms) after stimulus offset (Materials and Methods).

Thus, our conditional accuracy analysis allowed us to investigate quantitatively the second, STM-dependent stage in mouse visual perceptual dynamics. We estimated the duration over which above-chance decision accuracy is supported in mice after stimulus offset as  $\sim 1700$  ms (i.e.,  $t_{\text{chance}}$  minus the  $t_{\text{delay}}$ ).

### The presence of flanker stimulus modulates perceptual dynamics

We next investigated the impact of sensory context on visual decision dynamics. It is well established that the sensory context in which the perceptual target is presented modulates animals' behavior (Miller, 1991; Meier et al., 2011; Whitney and Levi, 2011). For instance, in the classic flanker task in humans, the co-occurrence of a flanker stimulus with conflicting information can interfere with perceptual performance (Eriksen and Eriksen, 1974; Fan et al., 2002). Recently, similar results were demonstrated in mice using a touchscreen version of the flanker task (You and Mysore, 2020). In this task (Fig. 4A), a target grating (always presented at the lower location) was accompanied by a flanker grating at the upper location with either orthogonal orientation ("incongruent" flanker) or same orientation ("congruent" flanker). Compared with the presence of a congruent flanker, the "incongruent" flanker significantly impaired discrimination accuracy (Fig. 4B, left;  $p < 0.001$ , paired-sample  $t$  test; effect size Hedges'  $g = 1.61$ ; re-plotted based on data from You and Mysore, 2020; Materials and Methods). Here, we analyzed that dataset with the conditional accuracy analysis to investigate whether an incongruent flanker affected the sensory encoding stage or the STM-dependent stage of perceptual dynamics.

To investigate the effect of the flanker on perceptual dynamics, we pooled trials from all mice into two groups based on their flanker congruency and sorted the trials based on their RT. Since previous study (You and Mysore, 2020) has demonstrated that the flanker affects performance significantly only when its luminance is higher than (or equal to) that of the target, here we included only high-luminance trials (trials with flanker luminance  $\geq 20.1$  cd/m<sup>2</sup>). To examine the sensory encoding stage quantitatively, we followed the approach used in Figure 2 and selected the trials on which mice responded before the stimulus ended (RT < 1000 ms), and aligned them to stimulus onset. Separately, to examine the STM-dependent stage, we followed the approach used in Figure 3 and selected the trials on which responses were made after the stimulus ended, and aligned them to stimulus offset.

The sensory encoding stage was significantly modulated by flanker congruency (Fig. 4C,D). We found that, the peak conditional accuracy for incongruent trials was

significantly lower than that of congruent trials (Fig. 4D, left;  $a_{\text{peak}}$ : congruent, median [C.I.] = 87.8 [86.3, 89.6] %, incongruent = 78.5 [76.9, 80.2] %; effect size (congruent-incongruent) Hedges'  $g = 11.0$ ), indicating that the presence of a high-luminance incongruent flanker interfered with the sensory encoding of the target stimulus. While the slope parameter for incongruent trials remains comparable to that of the congruent trials (Fig. 4D, middle; congruent = 11.9 [9.10, 15.5] a.u., incongruent = 15.3 [11.6, 20.6] a.u.; Hedges'  $g = -1.73$ ), the time to reach peak accuracy was, however, shorter for incongruent trials (Fig. 4D, right;  $t_{\text{peak}}$ : congruent = 413 [378, 458] ms, incongruent = 374 [340, 410] ms; Hedges'  $g = 2.08$ ), consistent with the lower  $a_{\text{peak}}$  (Fig. 4D, left).

The STM-dependent stage also appeared to be modulated by flanker congruency (Fig. 4E,F). Following stimulus offset, the time at which conditional accuracy dropped to chance was much earlier in incongruent trials than in congruent trials (Fig. 4F, right;  $t_{\text{chance}}$ : congruent, median [C.I.] = 2000 [1363, 2000] ms; incongruent = 1145 [816, 1985] ms; Hedges'  $g = 2.98$ ). However, this was likely due largely to the lower peak conditional accuracy for incongruent trials (Fig. 4F, left;  $a_{\text{peak}}$ : congruent = 84.5 [76.9, 88.6] %; incongruent = 75.9 [70.1, 82.1] %; Hedges'  $g = 2.54$ ), as opposed to changes in  $t_{\text{decay}}$  (Fig. 4F, middle; congruent = 299 [197, 1086] ms; incongruent = 343 [126, 802] ms; Hedges'  $g = 0.175$ ), or to the rate of decay (slope parameter; data not shown, congruent =  $-1.82$  [ $-10$ ,  $-1.0$ ] a.u., incongruent =  $-4.82$  [ $-10.0$ ,  $-1.60$ ] a.u.; Hedges'  $g = 0.99$ ).

In sum, we found that the presence of an incongruent flanker interferes the sensory encoding stage but not the STM-dependent stage of mouse visual decision dynamics.

### Stimulus onset delay modulates RT distribution but not the CAF

The components of behavioral performance that we have investigated thus far, namely, overall decision accuracy, RT distribution and CAF are related formally in the following way: the overall decision accuracy is the dot product of the CAF and RT distribution.

Our manipulations, thus far, produced changes in the CAF predominantly. Here, we wondered whether task parameters could, instead, alter RT distribution, and possibly do so without affecting the CAF. To test this, we added a delay between trial initiation and target onset (called stimulus onset delay) in the single-stimulus discrimination task. We reasoned that the extent to which mice are unable to adaptively withhold responding could impact the RT distribution.

We found that adding a stimulus onset delay did alter the RT distribution of mice (Fig. 5A, upper panel). The median RTs, measured relative to trial initiation, showed an increasing trend with delay (one-way ANOVA,  $p = 0.094$ ; effect size  $\eta^2 = 0.179$ ; Pearson's correlation = 0.422,  $p = 0.028$ ). This indicated that mice were able to sense the delayed onset of stimulus and thereby withhold their responses. However, mice were unable to withhold responding for the full duration required. By performing a linear regression

(Fig. 5A, upper panel, dashed line), we found that mice were able to withhold their responses for only 39 ms for every 100 ms of delay. Separately, this increase in RT for longer delays was accompanied by a trend toward lower decision accuracy (one-way ANOVA,  $p=0.182$ ; effect size  $\eta^2 = 0.132$ ; Pearson's correlation =  $-0.358$ ,  $p=0.067$ ; Fig. 5A, lower panel).

By contrast, conditional accuracy analysis revealed no effect of stimulus onset delay either on the sensory encoding stage (Fig. 5B,C,  $a_{\text{peak}}$ : no-delay, median [C.I.] = 84.2 [82.2, 86.4]%, 200-ms delay = 85.6 [82.9, 89.2]%, effect size (no-delay – 200-ms delay) Hedges'  $g = -1.12$ ; slope parameter: no-delay = 7.69 [5.82, 10.7] a.u., 200-ms delay = 6.61 [4.63, 8.74] a.u., Hedges'  $g = 0.264$ ;  $t_{\text{peak}}$ : no-delay = 494 [436, 557] ms, 200-ms delay = 552 [476, 680] ms, Hedges'  $g = -1.49$ ), or on the STM-dependent stage (Fig. 5D,E,  $a_{\text{peak}}$ : no-delay, median [C.I.] = 80.5 [75.6, 85.5]%, 200-ms delay = 80.9 [75.6, 84.9]%, Hedges'  $g = -0.147$ ;  $t_{\text{decay}}$ : no-delay = 976 [332, 1642] ms, 200-ms delay = 580 [319, 1585] ms, Hedges'  $g = 0.877$ ;  $t_{\text{chance}}$ : no-delay = 2214 [1865, 2400] ms, 200-ms delay = 2400 [1935, 2400] ms, Hedges'  $g = -1.22$ ).

Taken together, our results from varying the stimulus onset delay show that changes in RT distribution (and overall decision accuracy) are not necessarily accompanied by changes in the CAF. The observed trend of decreased accuracy was accounted for by the fact that with a delay, there were more responses initiated before the sensory encoding was complete, or even before the stimulus was presented (i.e., “impulsive” responses; Fig. 5B, histograms). To quantify such impulsivity, we propose an “impulsivity index” (ImpI):  $\text{ImpI} = 1 - \text{average (duration for which mice withhold responses/duration of the delay)}$ . Higher positive values of this index indicate greater impulsivity, with  $\text{ImpI} = 1$  indicating a complete inability to withhold responding in the face of stimulus delays (maximally impulsive). In the case of our mice,  $\text{ImpI}$  is  $\sim 0.6$  (see also Extended Data Fig. 5-1).

## Discussion

In this study, we quantify two distinct stages in the temporal dynamics of visual perceptual decisions in mice. First, a sensory encoding stage that is subject to the speed-accuracy trade-off, and then, a STM-dependent stage in which decision performance decays once the stimulus disappears. We also demonstrate that the CAF and the RT distribution can be affected independently by experimental manipulations. Whereas stimulus size, luminance, and presence of a foil modulate the CAF with minimal changes to the RT distribution, stimulus onset asynchrony modulates the RT distribution without changes to the CAF. Additionally, our results yield numerical estimates of fundamental psychophysical constants of visual perceptual decision-making in mice. Taken together, this study establishes a quantitative platform for future work dissecting neural circuit underpinnings of the dynamics of visually guided decision-making in mice.

## Estimates of time constants of the dynamics of visual perceptual decision-making in mice

Our results yielded numerical estimates of the duration of sensory encoding (i.e., the window of temporal integration) as 200–320 ms across stimulus size and luminance in mice (Fig. 2). This estimate is similar to that in humans: the internal representation of a visual stimulus is thought to be constructed within the first 200–300 ms of stimulus presentation (Shibuya and Bundesen, 1988; Busey and Loftus, 1994; Vogel et al., 2006; Bays et al., 2011). On the other hand, we also obtained an estimate of the duration of STM as 1700 ms. This constituted the period starting from stimulus offset to the last instant at which responses that are better than chance were initiated ( $t_{\text{chance}} - t_{\text{delay}} = \sim 1700$  ms; Fig. 3C). This duration does not necessarily represent just the maintenance of visual stimulus information in STM, it could also represent maintenance of information about the motor response associated with the stimulus (and likely, a combination of the two). Notably, our estimate of the duration of viability of the labile internal representation in mice falls in the same range as has been reported from human studies (Sperling, 1960; Posner and Keele, 1967; Phillips and Baddeley, 1971).

We have interpreted the decay in performance following stimulus offset as being because of loss of information in STM. A potential confounding factor to this interpretation is differences in the internal state of the animal, in selective attention, or more generally, task engagement. It is possible, for instance, that all the trials with longer RTs represent those in which mice did not pay attention to the stimulus (or more generally, were disengaged from the task), thereby being associated with lower accuracy. We believe this unlikely because attention/engagement was not varied systematically, here (unlike in the flanker task; Fig. 4). Even if loss of attention or engagement were a factor, any improvements in conditional accuracy because of increased attentiveness or engagement would only lengthen STM. From this perspective, our estimate of 1700 ms serves as a lower bound for the duration of STM.

This estimate of 1700 ms also represents a lower bound for working memory (WM). Whereas STM refers to the retention of information even when it is not accessible from the environment, WM refers additionally to the ability to manipulate this information and protect it from interference (Cowan, 2008; Postle and Pasternak, 2009). WM can be lengthened with training. For instance, in tasks that require animals hold information over an enforced delay period before responding, it has been reported that mice can learn to perform well with delay periods up to 5 s (Liu et al., 2014). Here, by allowing the natural evolution of the dynamics of decision-making to occur without an imposed delay period, we were able to estimate the “intrinsic” (lower bound for the) duration of STM.

## Estimates of the operating range of stimulus features for visual perceptual decision-making in mice

This study also yielded estimates for the range of values of various stimulus features within which mice are able to discriminate the visual target. The smallest stimulus size and lowest luminance (tested) at which mice were able to

discriminate orientation above chance were  $25^\circ$  and  $2.00 \text{ cd/m}^2$ , with mice performing at  $>80\%$  accuracy for most luminance values at that smallest size. The shortest stimulus that mice are able to discriminate above chance was  $\leq 100 \text{ ms}$  (Fig. 3A). Further, based on the x-intercept of the CAF in sensory encoding stage (median [C.I.] = 236 [215, 253] ms, pooling all trials of various sizes and luminance from Fig. 2), we were able to refine this estimate to be  $\leq 53 \text{ ms}$  (conservatively, after subtracting  $t_{\text{delay}} = \sim 200 \text{ ms}$ ). This is consistent to the estimation (40–80 ms) from a previous study based on visual cortical activity (Resulaj et al., 2018). In a subgroup of animals ( $n = 3$ ), we tested whether mice are able to discriminate orientation of the target stimulus ( $25^\circ$ ,  $0.1 \text{ cpd}$ ,  $16.2 \text{ cd/m}^2$ ) when it was 50 ms long. Two out of the three mice showed a response accuracy higher than chance (accuracy = 57.9%, 210 correct out of 363 trials,  $p = 0.002$ , binomial test; and 55.6%, 143/257,  $p = 0.040$ , respectively), consistent with this refined estimate. These findings that mice are able to discriminate visual stimuli in demanding sensory contexts suggest that the visual perceptual abilities of mice may be underrated.

The best discrimination performance reported in mice (accuracies  $>90\%$ ) have typically been obtained using large, often full-field, grating stimuli (Andermann et al., 2010; Long et al., 2015). In our single target discrimination task, the best performance ranged lower, between 75% and 90% (Fig. 1C), consistent with our use of “small” stimuli (relative to those typically used in mouse vision studies; Prusky et al., 2000; Prusky and Douglas, 2004; Wong and Brown, 2006; Busse et al., 2011; Long et al., 2015). Indeed, in our pilot study, the performance plateaued at  $\sim 93\%$  for a stimulus size  $\geq 45^\circ$  (Extended Data Fig. 1-1C,D). These results suggest that full-field stimuli may be effectively replaced by  $45^\circ$  stimuli to achieve best performance levels.

The best discrimination performance exhibited a dip at the highest luminance (Fig. 1C). This is potentially well accounted for by signal saturation: because the visual system adapts to the relevant range of stimulus luminance for best encoding (Ohzawa et al., 1982), the interleaved presentation of stimuli with different luminance can render the maximum-luminance stimulus unfavorable because of signal saturation (Long et al., 2015). Consistent with this idea, when the maximum-luminance stimulus ( $25^\circ$ ,  $0.1 \text{ cpd}$ ,  $130 \text{ cd/m}^2$ ) was presented *alone* in block design (Extended Data Fig. 1-1C, the black box at the left most, group median [C.I.] = 85.7 [77.6, 92.1] %), response accuracy was nominally higher than when it was presented interleaved with stimuli of varying luminance (Fig. 1C, the red box at the right most, group median [C.I.] = 79.7 [61.9, 91.9] %). These results indicate that a good upper bound for stimulus luminance in mouse experiments may be  $\sim 34 \text{ cd/m}^2$ .

### Stimulus and task parameters modulate perceptual performance through a variety of mechanisms

Increase in stimulus size and luminance both improved the overall discrimination performance of mice (Fig. 1). However, analysis of conditional accuracy revealed that

whereas increasing each increased the peak conditional accuracy ( $a_{\text{peak}}$ ), only increasing the stimulus luminance increased the slope of the CAF and resulted in a shorter  $t_{\text{peak}}$  (Fig. 2). We propose that these differences in the CAF reflect differential mechanisms at one or more levels of the underlying sensory processing. Specifically, in our experiments, varying stimulus luminance (through varying the intensity of just the bright phase of the grating) also varied stimulus contrast (relative to the dark background). On the other hand, increasing stimulus size increased the total luminance without affecting contrast. Consequently, differential activation of lateral inhibitory mechanisms for spatial contrast may account for the observed differences in CAFs. Separately, whereas increasing stimulus size and luminance both increase the total number of photons impinging on the retina, increasing stimulus size would activate a broader spatial distribution of photoreceptors (at a fixed signal-to-noise ratio), while increasing stimulus luminance would cause a largely fixed group of photoreceptors to receive a higher density of photons (and higher signal-to-noise ratio). Consequently, differential mechanisms of sensory integration (of the two) may also account for the observed differences in CAFs.

Separately, manipulating attention (by presenting a flanker) and manipulating the stimulus onset asynchrony both caused a reduction in response accuracy (Figs. 4B, 5A, lower panel). However, again, the analysis of conditional accuracy suggests that the mechanisms underlying the two are different: the capture of attention by the flanker interferes with the target's sensory encoding, whereas adding a prestimulus onset delay results in change of the RT distribution without affecting the CAF.

Taken together, our results demonstrate that although manipulating stimulus parameters or experimental conditions may induce seemingly similar changes in perceptual performance (overall accuracy), their underlying mechanisms could be different. The conditional accuracy analysis serves as an informative tool to explore these mechanisms and to understand the dynamics of perceptual decision-making.

### Qualitative differences between stimulus features as well as between task-difficulties

Across the various tasks and stimulus conditions that we studied here in mice, the sensory encoding stage ended rapidly, around 300 ms. However, in a recent study in which rats discriminated the direction of motion of a patch of random dots, the sensory encoding stage continued through at least 1.5 s (the longest RT bin reported; Shevinsky and Reinagel, 2019). We propose that this difference in the duration of sensory encoding may be because of fundamentally different nature of stimulus features used in these two studies. Consistent with this proposal, a study on human visual psychophysics (Burr and Santoro, 2001) has reported a temporal integration window of 200–300 ms when stimulus contrast of a patch of random dots was varied (similar to our results in mice), but a substantially longer integration window of 3 s when their motion coherence levels were varied (similar to the above-mentioned results in rats).

Separately, our results also highlight that “task difficulty” may be altered in qualitatively different ways, producing distinct outcomes on behavior. In the literature, task difficulty is often increased by making target stimuli more ambiguous or by introducing distracters (which we did also). Such manipulations often cause subjects (animals) to respond slower, allowing them time to gather more information to produce better performance (which we found, as well). However, when we shortened stimulus duration, which can plausibly be considered to also increase task difficulty, we found the opposite result, mice responded faster as the target stimulus became shorter (Fig. 3B). This potentially counterintuitive effect (faster RTs for a “more difficult” task) is explained well by the conditional accuracy analysis (Fig. 3C). Whereas shortening the stimulus duration makes the task more difficult, responding more slowly to shorter stimuli does not grant a perceptual benefit to the animals: once the stimulus has disappeared, withholding responses for longer would only increase the risk of losing information owing to memory decay. In other words, short stimuli impose a “time pressure” on animals to make decisions quickly. Thus, task difficulty may be altered in qualitatively different ways, with distinct behavioral effects.

### Optimal sensory sampling during visual perceptual decision-making in mice

An intriguing observation in our study is that across tasks, the peak of RT distribution (the RT bin with the largest number of trials) seemed to always occur around  $t_{\text{peak}}$  (Figs. 2A,C, 4C). Since the RT distribution can vary independently of the CAF (as demonstrated in Fig. 5), there is no a priori reason that the peak of RT distribution and the  $t_{\text{peak}}$  must change together. We propose that responding with RTs close to  $t_{\text{peak}}$  may be an optimal behavioral strategy for the mice. As indicated by the CAF, mouse response accuracy increased as RT increased until it reached a plateau at  $t_{\text{peak}}$ . Responding earlier than  $t_{\text{peak}}$ , therefore, would sacrifice accuracy, while responding later than  $t_{\text{peak}}$  would needlessly delay response (reducing the reward rate). Consequently, responding with the peak of RT distribution being equal to  $t_{\text{peak}}$  would be optimal. Testing this optimality hypothesis would require future experiments to manipulate the temporal integration window ( $t_{\text{peak}}$ ) substantially (much more than the 40- to 120 ms change we find in Figs. 2B,D, 4D), for instance, by manipulating stimulus coherence (Burr and Santoro, 2001) or the volatility of environment (Piet et al., 2018), and to ask whether this is accompanied by a commensurate shift in peak RT.

### References

- Andermann ML, Kerlin AM, Reid RC (2010) Chronic cellular imaging of mouse visual cortex during operant behavior and passive viewing. *Front Cell Neurosci* 4:3.
- Barrouillet P, Camos V (2012) As time goes by: temporal constraints in working memory. *Curr Dir Psychol Sci* 21:413–419.
- Bays PM, Gorgoraptis N, Wee N, Marshall L, Husain M (2011) Temporal dynamics of encoding, storage, and reallocation of visual working memory. *J Vis* 11:6.
- Brown J (1958) Some tests of the decay theory of immediate memory. *Q J Exp Psychol* 10:12–21.
- Burgess CP, Lak A, Steinmetz NA, Zatzka-Haas P, Bai Reddy C, Jacobs EAK, Linden JF, Paton JJ, Ranson A, Schröder S, Soares S, Wells MJ, Wool LE, Harris KD, Carandini M (2017) High-yield methods for accurate two-alternative visual psychophysics in head-fixed mice. *Cell Rep* 20:2513–2524.
- Burr DC, Santoro L (2001) Temporal integration of optic flow, measured by contrast and coherence thresholds. *Vision Res* 41:1891–1899.
- Busey TA, Loftus GR (1994) Sensory and cognitive components of visual information acquisition. *Psychol Rev* 101:446–469.
- Busse L, Ayaz A, Dhruv NT, Katzner S, Saleem AB, Schölvinck ML, Zaharia AD, Carandini M (2011) The detection of visual contrast in the behaving mouse. *J Neurosci* 31:11351–11361.
- Carandini M, Churchland AK (2013) Probing perceptual decisions in rodents. *Nat Neurosci* 16:824–831.
- Coltheart M (1980) Iconic memory and visible persistence. *Percept Psychophys* 27:183–228.
- Cowan N (2008) What are the differences between long-term, short-term, and working memory? *Prog Brain Res* 169:323–338.
- Dick A (1974) Iconic memory and its relation to perceptual processing and other memory mechanisms. *Percept Psychophys* 16:575–596.
- Eriksen BA, Eriksen CW (1974) Effects of noise letters upon the identification of a target letter in a nonsearch task. *Percept Psychophys* 16:143–149.
- Fan J, McCandliss BD, Sommer T, Raz A, Posner MI (2002) Testing the efficiency and independence of attentional networks. *J Cogn Neurosci* 14:340–347.
- Glickfeld LL, Histed MH, Maunsell JH (2013) Mouse primary visual cortex is used to detect both orientation and contrast changes. *J Neurosci* 33:19416–19422.
- Glickfeld LL, Reid RC, Andermann ML (2014) A mouse model of higher visual cortical function. *Curr Opin Neurobiol* 24:28–33.
- Gold JM, Murray RF, Sekuler AB, Bennett PJ, Sekuler R (2005) Visual memory decay is deterministic. *Psychol Sci* 16:769–774.
- Guo ZV, Hires SA, Li N, O'Connor DH, Komiyama T, Ophir E, Huber D, Bonardi C, Morandell K, Gutnisky D, Peron S, Xu NL, Cox J, Svoboda K (2014) Procedures for behavioral experiments in head-fixed mice. *PLoS One* 9:e88678.
- Heitz RP (2014) The speed-accuracy tradeoff: history, physiology, methodology, and behavior. *Front Neurosci* 8:150.
- Hentschke H, Stüttgen MC (2011) Computation of measures of effect size for neuroscience data sets. *Eur J Neurosci* 34:1887–1894.
- Histed MH, Maunsell JH (2014) Cortical neural populations can guide behavior by integrating inputs linearly, independent of synchrony. *Proc Natl Acad Sci USA* 111:E178–E187.
- Histed MH, Carvalho LA, Maunsell JH (2012) Psychophysical measurement of contrast sensitivity in the behaving mouse. *J Neurophysiol* 107:758–765.
- Huberman AD, Niell CM (2011) What can mice tell us about how vision works? *Trends Neurosci* 34:464–473.
- Liu D, Gu X, Zhu J, Zhang X, Han Z, Yan W, Cheng Q, Hao J, Fan H, Hou R, Chen Z, Chen Y, Li CT (2014) Medial prefrontal activity during delay period contributes to learning of a working memory task. *Science* 346:458–463.
- Long M, Jiang W, Liu D, Yao H (2015) Contrast-dependent orientation discrimination in the mouse. *Sci Rep* 5:15830.
- Mar AC, Horner AE, Nilsson SR, Alsiö J, Kent BA, Kim CH, Holmes A, Saksida LM, Bussey TJ (2013) The touchscreen operant platform for assessing executive function in rats and mice. *Nat Protoc* 8:1985–2005.
- McElree B, Doshier BA (1989) Serial position and set size in short-term memory: the time course of recognition. *J Exp Psychol Gen* 118:346–373.
- Meier P, Flister E, Reinagel P (2011) Collinear features impair visual detection by rats. *J Vis* 11:22–22.

- Miller J (1991) The flanker compatibility effect as a function of visual angle, attentional focus, visual transients, and perceptual load: a search for boundary conditions. *Percept Psychophys* 49:270–288.
- Nomura Y, Ikuta S, Yokota S, Mita J, Oikawa M, Matsushima H, Amano A, Shimonomura K, Seya Y, Koike C (2019) Evaluation of critical flicker-fusion frequency measurement methods using a touchscreen-based visual temporal discrimination task in the behaving mouse. *Neurosci Res* 148:28–33.
- Ohzawa I, Sclar G, Freeman RD (1982) Contrast gain control in the cat visual cortex. *Nature* 298:266–268.
- Phillips W, Baddeley A (1971) Reaction time and short-term visual memory. *Psychon Sci* 22:73–74.
- Piet AT, El Hady A, Brody CD (2018) Rats adopt the optimal time-scale for evidence integration in a dynamic environment. *Nat Commun* 9:4265.
- Posner MI, Keele SW (1967) Decay of visual information from a single letter. *Science* 158:137–139.
- Postle B, Pasternak T (2009) Short term and working memory. In: *Encyclopedia of neuroscience*, pp 783–789. San Diego: Elsevier.
- Prusky GT, Douglas RM (2004) Characterization of mouse cortical spatial vision. *Vision Res* 44:3411–3418.
- Prusky GT, West PW, Douglas RM (2000) Behavioral assessment of visual acuity in mice and rats. *Vision Res* 40:2201–2209.
- Ratcliff R (1978) A theory of memory retrieval. *Psychol Rev* 85:59–108.
- Ratcliff R, Smith PL, Brown SD, McKoon G (2016) Diffusion decision model: current issues and history. *Trends Cogn Sci* 20:260–281.
- Resulaj A, Ruediger S, Olsen SR, Scanziani M (2018) First spikes in visual cortex enable perceptual discrimination. *Elife* 7:e34044.
- Ricker TJ, Vergauwe E, Cowan N (2016) Decay theory of immediate memory: from Brown (1958) to today (2014). *Q J Exp Psychol (Hove)* 69:1969–1995.
- Seabrook TA, Burbridge TJ, Crair MC, Huberman AD (2017) Architecture, function, and assembly of the mouse visual system. *Annu Rev Neurosci* 40:499–538.
- Shevinsky CA, Reinagel P (2019) The interaction between elapsed time and decision accuracy differs between humans and rats. *Front Neurosci* 13:1211.
- Shibuya H, Bundesen C (1988) Visual selection from multielement displays: measuring and modeling effects of exposure duration. *J Exp Psychol Hum Percept Perform* 14:591–600.
- Siegel M, Engel AK, Donner TH (2011) Cortical network dynamics of perceptual decision-making in the human brain. *Front Hum Neurosci* 5:21.
- Smith PL, Ratcliff R (2009) An integrated theory of attention and decision making in visual signal detection. *Psychol Rev* 116:283–317.
- Speed A, Del Rosario J, Mikail N, Haider B (2020) Spatial attention enhances network, cellular and subthreshold responses in mouse visual cortex. *Nat Commun* 11:505.
- Sperling G (1960) The information available in brief visual presentations. *Psychol Monogr* 74:1–29.
- Stanford TR, Shankar S, Massoglia DP, Costello MG, Salinas E (2010) Perceptual decision making in less than 30 milliseconds. *Nat Neurosci* 13:379–385.
- Steinemann NA, O’Connell RG, Kelly SP (2018) Decisions are expedited through multiple neural adjustments spanning the sensorimotor hierarchy. *Nat Commun* 9:3627.
- Thura D, Cisek P (2014) Deliberation and commitment in the premotor and primary motor cortex during dynamic decision making. *Neuron* 81:1401–1416.
- Uchida N, Kepecs A, Mainen ZF (2006) Seeing at a glance, smelling in a whiff: rapid forms of perceptual decision making. *Nat Rev Neurosci* 7:485–491.
- Umino Y, Pasquale R, Solessio E (2018) Visual temporal contrast sensitivity in the behaving mouse shares fundamental properties with human psychophysics. *eNeuro* 5:ENEURO.0181-18.2018.
- Vogel EK, Woodman GF, Luck SJ (2006) The time course of consolidation in visual working memory. *J Exp Psychol Hum Percept Perform* 32:1436–1451.
- Voss A, Nagler M, Lerche V (2013) Diffusion models in experimental psychology: a practical introduction. *Exp Psychol* 60:385–402.
- Voss A, Voss J, Lerche V (2015) Assessing cognitive processes with diffusion model analyses: a tutorial based on fast-dm-30. *Front Psychol* 6:336.
- Wang L, Krauzlis RJ (2018) Visual selective attention in mice. *Curr Biol* 28:676–685.e4.
- Whitney D, Levi DM (2011) Visual crowding: a fundamental limit on conscious perception and object recognition. *Trends Cogn Sci* 15:160–168.
- Wickelgren WA (1977) Speed-accuracy tradeoff and information processing dynamics. *Acta Psychol* 41:67–85.
- Wilming N, Murphy PR, Meyniel F, Donner TH (2020) Large-scale dynamics of perceptual decision information across human cortex. *Nat Commun* 11:5109.
- Wong AA, Brown RE (2006) Visual detection, pattern discrimination and visual acuity in 14 strains of mice. *Genes Brain Behav* 5:389–403.
- Yang Y, DeWeese M, Otazu G, Zador A (2008) Millisecond-scale differences in neural activity in auditory cortex can drive decisions. *Nat Neurosci* 11:1262–1263.
- You WK, Mysore SP (2020) Endogenous and exogenous control of visuospatial selective attention in freely behaving mice. *Nat Commun* 11:1986.
- Zariwala HA, Kepecs A, Uchida N, Hirokawa J, Mainen ZF (2013) The limits of deliberation in a perceptual decision task. *Neuron* 78:339–351.
- Zhang W, Luck SJ (2009) Sudden death and gradual decay in visual working memory. *Psychol Sci* 20:423–428.